Acupuncture at Hegu (IC4) Point Detects Brain Oxygen Supply Disturbances in Patients with Brain Disorders: a fNIRS study on brain oxygen sensing

Prof.Dr.med.Helmut Acker

FNG.do@t-online.de

Forschungsinstitut für Notfallmedizin und Gesundheit (FONOG, UG), Kuntzestr. 59, D-44225 Dortmund, Germany https://orcid.org/0000-0001-5589-5508

Dr.med. Wilhelm Ehleben

Forschungsinstitut für Notfallmedizin und Gesundheit (FONOG, UG), Kuntzestr. 59, D-44225 Dortmund, Germany

Dr.rer.nat. Jörn M. Horschig

Artinis Medical Systems B.B.; Einsteinweg 17, 6662 PW Elst, Netherlands

Case Report

Keywords: acupuncture, functional near-infrared spectroscopy, O2Hb, HHb, brain oxygen supply, neurovascular coupling, mitochondrial oxygen sensing, EEG Fourier power analysis, brain disorder, Alzheimer´s disease, artificial neural network

Posted Date: July 23rd, 2024

DOI: https://doi.org/10.21203/rs.3.rs-4764825/v1

Additional Declarations: The authors declare no competing interests.

Abstract

The functional near infrared spectroscopy (fNIRS) technique was introduced for use in general medical practice to measure brain blood oxygenation along with physiological parameters such as 4-channel EEG, heart rate, blood oxygenation, blood volume changes and autonomic nerve activity. An artificial neuronal network was used to adjust the brain blood oxygenation measurements to evaluate changes in these physiological parameters. Early detection of cerebral blood flow disorders related to cognitive impairments such as Alzheimer´s disease appears to be feasible. Acupuncture with Hegu (LI4) was applied to stimulate brain neuronal networks in 5 control patients (CPs) and 5 brain disorder patients (BDPs). The following conclusions were drawn:

1. fNIRS recordings of brain hemoglobin oxygenation indicate the efficacy of brain microcirculation and brain oxygen supply

2. Central brain acupuncture stimulation reveals deficits in the brain microcirculation and oxygen supply of BDPs

3. A 20-second period of acupuncture stimulation results in brain hypoxia in BDPs but not in CPs, primarily due to mismatching of arterial and venous microcirculation

4. fNIRS combined with subsequent ANN analysis of brain oxygen supply could be very effective and user friendly for recording early signs of brain microcirculation dysregulation and therapeutic progress.

Introduction

In general, in medicine, people are being increasingly confronted with elderly people suffering from dementia related to Alzheimer´s disease, including poststroke or traumatic brain disorders (Raz et al., 2016). Early detection of mild cognitive impairment by functional near infrared spectroscopy (fNIRS) is crucial for initiating medical interventions (Srinivasan et al., 2023). To aid in this, we developed an application for measuring blood oxygenation status to identify disorders of cerebral blood flow, as previously described (Ehleben et al., 2023). Cerebral blood flow is influenced by physiological parameters such as heart rate (HR), blood volume changes (Pleth), hemoglobin oxygen saturation (SaO2), autonomic nervous system activity (GSR), and neural cell activity (Li Rihui et al., 2019). We measured these physiological parameters along with four bipolar EEG recordings (see Fig. 1) simultaneously with fNIRS in patients. Fourier power analysis yielded 23 parameters for analyzing the fNIRS signal concerning cerebral and extracerebral oxygenation factors (Ehleben et al., 2023). The significance of each parameter for the fNIRS signal was evaluated using an artificial neural network (ANN), which is recognized for nonlinear regression analysis of large medical datasets (B. Richards, D. Tsao, 2022). Additionally, O_2Hb-HHb relation plots were created to analyze brain oxygen supply regulation.

We applied fNIRS to 5 healthy control patients (CPs) and 5 patients with brain disorders (BDPs), such as Alzheimer’s disease, which is known to cause disturbed neurovascular coupling (NVC) (Mamelak, 2023).

Various acupuncture points, including the Hé gǔ (Hegu, Union Valley, Large intestine meridian 4) (Andrew Ellis, 1989), have demonstrated benefits in stroke rehabilitation by promoting neurogenesis and cell proliferation, regulating cerebral blood flow, preventing apoptosis, modulating neurochemicals, and improving impaired long-term potentiation and memory (Chavez et al., 2017).

fNIRS with ANN analysis and O_2Hb-HHb relation plots revealed significant differences between CPs and BDPs due to the varying impact of the 23 parameters on the kinetics of oxygenated and deoxygenated blood. The effect of Hegu acupuncture is comparable to the O_2Hb-HHb relationships observed under other NVC stimulations, such as touch, smell, taste, music, or calculations (Ehleben et al., 2023). These types of studies need to be supplemented with additional patients utilizing O_2Hb-HHb relationships as early indicators of impaired NVC function in patients with BDPs (Mamelak, 2023) or monitoring therapeutic success in the early treatment of cognitive deficiencies in general medical practice.

Materials and Equipment

Figure 1 shows a schematic representation of the head cap configuration, as previously described (Ehleben et al., 2023); this configuration combines the 8-channel fNIRS OCTAMON device (manufactured by Artinis Medical Systems B. V, Elst, Netherlands) and the Bluetooth-enabled EEG TMSiMobi 6-channel amplifier (produced by TMSi, Oldenzaal, Netherlands). The fNIRS system utilizes multiple optodes (OCTAMON) primarily attached to the frontal region of the head. Eight transmitter diodes (Tx1-Tx4 on the right side and Tx5-Tx8 on the left side of the frontal head) emit light at wavelengths of approximately 751 nm and 843 nm, respectively, to measure the kinetics of HHb and O_2Hb for assessing neurovascular coupling (NVC) and cerebral blood flow autoregulation (Oldag et al., 2016). Near-infrared light within this wavelength range is predominantly absorbed by hemoglobin and to a lesser extent by water and lipids (Davies et al., 2015). The emitted fNIRS light penetrates brain tissue to a depth of 23 mm, with the deepest 5% reaching the gray cerebral tissue and 17.4% reaching a depth of 20.3 mm, indicating that a significant portion of the emitted light contains information about extracerebral regions such as the skin, bone, and muscles (Haeussinger et al., 2011). The fNIRS light is detected by two receivers, Rx1 and Rx2, after traversing the brain tissue, enabling the determination of O_2Hb and HHb levels in the blood using a modified Lambert–Beer law. Additionally, four bipolar EEG signals (F3-F4, C3-C4, Fz-Oz, and P3-P4), the GSR for measuring autonomic nervous system activity, heart rate (HR), and arterial oxygen saturation (SaO2) using photoplethysmography (Pleth), as well as blood volume changes in a fingertip, were recorded at a rate of 256 Hz using the TMSiMobi system. The simultaneous measurement of various anatomical and physiological parameters during fNIRS registration, along with their identification in the fNIRS signal, is essential for obtaining a comprehensive understanding of NVC for review (see)cholkmann et al., 2022). However, the interpretation of fNIRS signals in relation to NVC under different neuronal stimulation conditions is restricted by anatomical and physiological interference (Agbangla et al., 2017). The sampling rate of the fNIRS system was set at 50 Hz, but the data were upsampled to match the 256 Hz sampling rate of the other devices. The OxySoft program (Artinis

Medical Systems B. V., Elst, Netherlands) was used for data recording, visualization, and computation. The collected data were stored in Excel files (Microsoft) for further analysis.

Patients

Ten patients who regularly consulted a general medicine practice linked to FONOG (more information: www.fonog.de) were offered brain oxygen supply control using fNIRS. Five patients (mean age 45 ± 10 y) without brain disorders served as the control group (CPs), while five patients (mean age 62 ± 22 y), including three with Alzheimer's disease (ICD10 G30.9, mean age 74 ± 8 y), one who experienced a stroke episode (ICD10 I69.4, age 69 y), and one with autism (ICD10 F84.1, age 24 y), served as examples of brain disorder patients (BDPs). There were no statistically significant differences in age between the two groups ($p > 0.05$). The patients provided written informed consent for the use of their data in this publication using the Patient Consent Form Template (https://www.medizininformatik-initiative.de/). The institutional ethics committee of Ärztekammer Westfalen Lippe (Münster, Germany) was informed about the use of patient data for this study (2023-199-f-S).

EEG time-frequency analysis

The EEG time series were processed as follows: First, detrending was performed by subtracting the least-squares fit of a straight line from the data. This procedure was used to remove any linear trend from the time series. Next, the time-frequency representation of the detrended data was obtained using the short-time Fourier transform. A Hamming window of 128 points with a 50% overlap was applied to the data during the transformation. This allowed for the analysis of the temporal variations in the frequency content of the EEG signals. To facilitate the visualization and analysis of the resulting spectrum, the amplitude values were converted to decibels (dB). This conversion provides a logarithmic representation of the amplitude, which can better capture the dynamic range of the EEG signals. To standardize the time-frequency representation, it was interpolated to a frequency of 256 Hz. This interpolation allowed for a uniform time-frequency resolution across the entire spectrum. Finally, the mean amplitude for specific EEG bandwidths was computed. These bandwidths, which are commonly used in EEG analysis, include delta (1–4 Hz), theta (4–8 Hz), alpha (8–13 Hz), beta (14–30 Hz), and gamma (30–100 Hz) bands. The mean amplitude values were calculated for bipolar EEG recordings, which involve the measurement of electrical potential differences between two specific electrode placements. This provides information about the activity within specific brain regions or networks at different frequency ranges.

NVC stimulation by acupuncture

During the experimental session, patients were instructed to rest for a period of 10 minutes in a comfortable chair to acclimate to the fNIRS-EEG head cap. Acupuncture was subsequently performed according to a previously described methodology (Acker et al., 2015). Specifically, single sterile steel needles measuring 0.22x13 mm (brand: Gushi-zhengzheng, Medical Device, Henang, China) were utilized for the acupuncture procedure. Prior to the insertion of the needle, the Hegu acupuncture point, as

depicted in Fig. 1, was thoroughly disinfected. The needle was then superficially inserted into the skin approximately 5 mm deep by a medical doctor qualified as a consultant for acupuncture. Subsequently, the needle was gently rotated in a clockwise direction for a duration of 20 seconds until the rotation was impeded by tissue resistance.

Statistics

The data analysis began 10 seconds prior to the start of the 20-second acupuncture session. The fNIRS data were normalized, and the analysis continued for approximately 30–40 seconds after the completion of the acupuncture. A t test was performed to compare the differences in recordings between the CP group (n = 5) and the BDP group (n = 5). The impact of the 23 parameters on brain O2Hb and HHb levels was assessed. The normality of the distribution of the data was controlled for using a probability-probability (PP) test conducted in IBM SPSS Statistics version 27. The level of statistical significance was set at an alpha error level of $p < 0.05$. Graphs were created using Microsoft Excel and PowerPoint.

The relative importance—comparable to the standardized beta coefficient of linear regression—of the 23 parameters for recalculating O_2Hb and HHb reactions to acupuncture NVC stimulation was assessed by ANN nonlinear regression (see Fig. 4) composed of a 1-neural layer containing up to 18 units called the hidden layer (blue), 1 input layer containing the 23 explanatory parameters (left side) and 1 output layer containing the fNIRS-measured oxygenation variables (right side, Multilayer Perceptron Network, IBM SPSS Statistics, Armonk, NY software version 27). Approximately 70% of the measured parameter values were used for training the ANN. The subsequent testing by the ANN used 30% of the measured parameter values. The training and testing times were approximately 3 seconds, and the mean relative error of recalculation was 0.057 ± 0.017 for CPs and 0.031 ± 0.01 for BDPs ($p < 0.05$).

The English language and grammar were managed by **the** AJE Orcid Curie feature.

Results

As shown in Fig. 2, on the right side, O_2 Hb and HHb reactions to right-hand Hegu acupuncture (event) were observed for 20 seconds in the Pat04 BD patient. These measurements were conducted using frontal head fNIRS of Tx1-Tx8 O_2 Hb (red) and HHb (blue) patients, as well as simultaneous registrations of bipolar EEGs (black, F3-F4, C3-C4, Fz-Oz, P3-P4). The figure below shows the simultaneous changes in SaO_2, HR, GSR, and Pleth during the same time period.

Figure 2 shows O_2Hb and HHb reactions to right-hand Hegu acupuncture (event) for 20 s on the left side of the Pat05 CP as measured by frontal head fNIRS of Tx1-Tx8 O_2Hb (red) and HHb (blue) as well as simultaneous registrations of bipolar EEGs (F3-F4, C3-C4, Fz-Oz, P3-P4). The figure below shows the changes in SaO_2, HR, GSR, and platelet count during the same time period. The data analysis generally started 10 s before the onset of NVC stimulation by acupuncture. O_2Hb starts to increase, and HHb decreases approximately 10 s after acupuncture (event) is terminated. Concomitantly, EEG activity

increased significantly in F3-F4. The figure below shows some SaO_2 oscillations, while HR decreases a typical acupuncture reaction (Acker et al., 2015), probably due to a decrease in the GSR indicating sympathetic tone loss. Pleth shows increasing blood volume changes, most likely superimposed with various frequency components attributed to respiration, sympathetic nervous system activity and thermoregulation (Allen, 2007). Figure 2 shows O_2Hb and HHb reactions to right-hand Hegu acupuncture (event) for 20 s on the right side of BD Pat04 as measured by frontal head fNIRS of Tx1-Tx8 O2Hb (red) and HHb (blue) as well as simultaneous registrations of bipolar EEGs (F3-F4, C3-C4, Fz-Oz, P3-P4). O_2Hb decreases in response to acupuncture (event), and HHb increases correspondingly. Acupuncture is followed by enhanced EEG activity in all recordings. The figure below shows simultaneous changes in SaO_2, HR, GSR, and Pleth during the same time period. Whereas SaO_2 oscillates, HR finally decreases, and GSR shows corresponding sympathetic tone loss periods. The pleth remains stable in the first phase and continues to increase with increasing blood volume.

Figure 3A shows the O_2Hb reactions of channels T1-Tx8 from 5 CPs to acupuncture for 20 s (shaded area) as gray lines. The values for CP05 are shown as dotted gray lines. The mean O_2Hb reaction is shown as a solid black bold line, whereas the mean HHb reaction is shown as a broken black bold line. Figure 3B shows the single O_2Hb reactions of channels T1-Tx8 of 5 BDPs to acupuncture for 20 s (shaded area) as gray lines. The values of BDP 04 are shown as dotted gray lines. The mean O_2Hb reaction is shown as a solid black bold line, whereas the mean HHb reaction is shown as a broken black bold line. The mean O_2Hb reaction and mean HHb reaction of CPs and BDPs were significantly different ($p < 0,05$), indicating an increase in the brain oxygen supply of CPs and an impairment of the oxygen supply of BDPs under acupuncture at Hegu.

Figure 4 shows the differences in brain oxygen supply in response to Hegu acupuncture between CPs and BDPs. The x-axis shows the O_2Hb, and the y-axis shows the corresponding HHb optical density (OD) changes as the mean value of 5 CPs (black solid line) and 5 BDPs (gray solid line). The bold part of the lines represents the time period of 20 s of acupuncture. CPs dominate with their meandering increasing O_2Hb and decreasing HHb values, indicating that microcirculation likely regulates brain oxygen supply. BDPs contrast with nearly linear decreases in O_2Hb and increases in HHb, indicating microcirculation impairment during acupuncture-induced brain hypoxia. The question was whether this difference could be explained by the different importance of the 23 parameters measured and calculated for the fNIRS oxygenation recordings (see Fig. 2). Figure 5 highlights this aspect.

Figure 6 shows the ANN setup for analyzing the relative importance of 23 measured explanatory parameters (left side of the blue part) for estimating the Tx1-Tx8 O_2Hb- and HHb-dependent variables (right side of the blue part) under acupuncture using one hidden neural layer with 18 units (blue middle part). The left panel shows the 23 explanatory parameters measured and calculated during the experiment and their relative importance used for recalculation. *The diagrams on the right side of the blue part* show the linear relationship between the measured and ANN-recalculated Tx4 O_2Hb of 1 CP (Pat05) and Tx4 O_2Hb values for 1 BDP (Pat04) and the corresponding relative error. The relative error of

the calculations for the BDP recordings was significantly lower than that for the CP recordings, likely suggesting a reduced and more linear influence of the 23 explanatory parameters.

Figure 7 shows a net diagram of the relative importance of 23 parameters for recalculating fNIRS O_2Hb (black line) and HHb changes (gray line) upon Hegu acupuncture for 20 s for 5 CPs (left side) and 5 BDPs (right side). Peripheral factors such as HR and the GSR are highly important for recalculating fNIRS O_2Hb changes in CPs and BDPs. Various brain power activities, as measured by EEG, are dominant for recalculating fNIRS O_2Hb changes in BDPs. Interestingly, net diagram analysis for BDPs revealed a significant difference between O_2Hb and HHb changes in contrast to those in CPs, indicating perhaps a mismatch of arterial and venous microcirculation control leading to brain hypoxia, as shown in Figs. 2, 3, and 4.

Discussion

The direct stimulatory effect of acupuncture on central nervous system structures results in immediate changes in the limbic-paralimbic neocortical network, as measured by BOLD (blood oxygenation level-dependent) fMRI. These networks closely match the task-negative default mode network and the anti-correlated task-positive network as afferent targets (Acker et al., 2015). Acupuncture can change the structural characteristics and functionality of synaptic plasticity by modulating synaptic proteins, inhibiting inflammatory responses in neural pathways, increasing mitochondrial energy metabolism, and decreasing amyloid beta deposition; for a review, see (Du et al., 2022).

Cerebral blood flow (CBF) regulation is essential for normal brain function. The mammalian brain has evolved a unique mechanism for CBF control known as NVC. This mechanism ensures a rapid increase in the rate of CBF and oxygen delivery to activated brain structures. The NVC unit is composed of astrocytes, mural vascular smooth muscle cells, pericytes, and endothelial cells and regulates neurovascular coupling. A decrease in cerebral blood flow is the earliest change to occur in AD and is generated at the capillary level. Changes in the capillary control of CBF correlate with cognitive decline. The reduction in CBF produced by pericytes constricting capillaries, along with subsequent decreases in CBF as a result of capillary occlusion by neutrophils and thrombi, is an important dysfunction in AD. Initial evidence indicates that reversing this reduction in CBF can restore cognitive function, provided that damage to synapses, neurons and circuits has not advanced significantly for review (Korte et al., 2020). Consequently, the fNIRS screening ANN test, as described (Ehleben et al., 2023), might allow early detection and therapeutic intervention to maintain CBF as a key aim for the future treatment of AD and related brain disorders.

Epidemiologic studies indicate that approximately one-third of patients with AD present vascular pathology, indicating that a strong vascular component induces diminished cerebral blood flow followed by hypoxia and a leaky blood brain barrier (Raz et al., 2016). Studies in the living human brain have established that aberrant cerebrovascular reactivity, CBF reductions and dysregulated CBF are prominent features during the early stages of disease across the aging–mild cognitive impairment–AD spectrum

(Kisler et al., 2017). Deterioration of the brain's microvasculature, particularly in the hippocampal memory center, appears to be a very early event in the development of AD preceding even the deposition of amyloid-beta (Aβ). A damaged microvasculature reduces the supply of oxygen and glucose to this region, and mitochondrial damage might additionally limit ATP production. This damage may be a function of the early increase in the expression and activity of NADPH oxidase (NOX) in the endothelial cells of microvessels with age (Mamelak, 2023). The cause of AD-related mitochondrial dysfunction could be amyloid (Aβ) cascade-induced mitochondrial dysfunction. However, other data indicate that mitochondrial dysfunction is independent of Aβ, suggesting the occurrence of a primary mitochondrial cascade. Mitochondria, therefore, at least appear to mediate Aβ or possibly even initiate pathologic molecular cascades in AD (Swerdlow, 2018). Aβ mainly disturbs the functions of complexes I and IV of the respiratory chain. An increase in N1-methylation of adenosine (m^1A) of ND5 mRNA might lead to dysfunction of mitochondrial complex I in an AD cell model as well as in AD patients. These findings suggest that a newly identified mechanism is likely involved in Aβ-induced mitochondrial dysfunction (Jörg et al., 2024) (Monzio Compagnoni et al., 2020). Analyses of the associations of the activities of complexes I, II, III, and IV and citrate synthase (CS) with disease severity in patients with major depressive disorder (MDD) or Alzheimer's disease (AD) were performed for both AD and MDD patients. However, the mean values of mitochondrial parameters were significantly altered in AD patients but not in MDD patients. In AD, a decrease in the activity of CS and complex IV may cause mitochondrial dysfunction, whereas an increase in the activity of other mitochondrial complexes or their ratios to CS may be an adaptive response (Fišara et al., 2019).

These various NVC responses might be based not only on neuronal brain activity but also on a range of oxygen-sensing signaling cascades (Acker and Acker, 2004) regulating CBF, as shown in Fig. 8.

Carotid body (CB) NADPH oxidase, mitochondrial complex I and complex IV of CB type I cells are the most likely oxygen sensor candidates for initiating hypoxia-induced release of neurotransmitters (NTs) to excite synaptically connected sinus nerve fibers to regulate ventilation and blood circulation centers in the brainstem. Stimulation of NADPH oxidase by enhanced p47 binding decreases sinus nerve activity, and poisoning complex I silences sinus nerve activity. Complex IV contains four redox centers, namely, heme a and heme a3, which are linked by helix X and two copper centers (CuA and CuB). Oxygen binds to the haem a3-CuB binuclear center, and helix-X stretches, facilitating communication between the two haem groups and enhancing electron transfer from mitochondrial cytochrome c (complex III) over CuA to haem a and the binuclear center. The shape of the intracellular mitochondrial network changes by approximately 3 Å upon helix-X movement, presumably inducing a change in cell shape with variations in the activity of stretch-sensitive ion channels (Acker and Fandrey, 2022)). Assuming that the CB oxygen sensor mechanism might also be valid for brain NVC regulation, Fig. 8 proposes that the regulatory neuron signal is controlled by oxygen sensors to optimize CBF and the blood supply in the brain. Assuming that one of the oxygen sensor candidates is NADPH oxidase, complexes I and IV are defective, as described for AD-linked brain disorders ((Mamelak, 2023)(šar et al., 2019)(Jörg et al., 2024) brain microcirculation is dysregulated, as shown in Fig. 4,7, due to a mismatch of arterial and venous

perfusion. This mismatch resulting in brain hypoxia was also observed in BDPs confronted with tasks such as calculation, smelling, tasting or music (Ehleben et al., 2023).

Declarations

Declaration of Interests:

The authors declare that there are no conflicts of interest regarding the publication of this article.

Acknowledgments:

We thank Gisela Acker for her generous private financial support of the project and Sofia Sappia for her excellent contribution by establishing the EEG Fourier analysis.

References

1. Acker H, Fandrey J, Carotid body physiology meets cytochrome c oxidase crystallography Commentary to Ortega-Sáenz, López-Barneo P, Torres-Torrelo J, Ortega-Sáenz H, Gao P (2022) L, López-. Pflugers Arch 474, 187–189. https://doi.org/10.1007/s00424-021-02662-8
2. Acker H, Schmidt-Rathjens C, Acker T, Fandrey J, Ehleben W (2015) Acupuncture–brain interactions as hypothesized by mood scale recordings. Med Hypotheses 85:371–379. https://doi.org/10.1016/j.mehy.2015.05.013
3. Acker T, Acker H (2004) Cellular oxygen sensing need in CNS function: physiological and pathological implications. J Exp Biol 207:3171–3188. https://doi.org/10.1242/jeb.01075
4. Agbangla NF, Audiffren M, Albinet CT (2017) Use of near-infrared spectroscopy in the investigation of brain activation during cognitive aging: A systematic review of an emerging area of research. Aging Res Rev 38:52–66. https://doi.org/10.1016/j.arr.2017.07.003
5. Allen J (2007) Photoplethysmography and its application in clinical physiological measurement. Physiol Meas. https://doi.org/10.1088/0967-3334/28/3/R01
6. Andrew Ellis NWKB (1989) GRASPING THE WIND. Paradigma, Brookline Massachusetts
7. Richards B, Tsao D, A.Z (2022) The application of artificial intelligence to biology and neuroscience. Cell 05:2640–2643
8. Chavez LM, Huang SS, MacDonald I, Lin JG, Lee YC, Chen YH (2017) Mechanisms of acupuncture therapy in ischemic stroke rehabilitation: A literature review of basic studies. Int J Mol Sci. https://doi.org/10.3390/ijms18112270
9. Davies DJ, Su Z, Clancy MT, Lucas SJE, Dehghani H, Logan A, Belli A (2015) Near-Infrared Spectroscopy in the Monitoring of Adult Traumatic Brain Injury: A Review. J Neurotrauma 32:933–941. https://doi.org/10.1089/neu.2014.3748

10. Du K, Yang S, Wang J, Zhu G (2022) Acupuncture Interventions for Alzheimer's Disease and Vascular Cognitive Disorders: A Review of Mechanisms. Oxid Med Cell Longev. https://doi.org/10.1155/2022/6080282
11. Ehleben W, Horschig JM, Acker H (2023) Artificial Neural Network Analysis of Prefrontal fnirs Blood Oxygenation Recordings Affiliation. Archives Intern Med Res 6:116–128. https://doi.org/10.26502/aimr.0156
12. Fišar Z, Hansika H, Křížová J, Jirák R, Kitzlerová E, Zvěřová M, Hroudová J, Wenchich L, Zeman J, Raboch J (2019) Activities of mitochondrial respiratory chain complexes in platelets of patients with Alzheimer's disease and depressive disorder. Mitochondrion 48:67–77. https://doi.org/10.1016/j.mito.2019.07.013
13. Haeussinger FB, Heinzel S, Hahn T, Schecklmann M, Ehlis AC, Fallgatter AJ (2011) Simulation of near-infrared light absorption considering individual head and prefrontal cortex anatomy: Implications for optical neuroimaging. PLoS ONE 6. https://doi.org/10.1371/journal.pone.0026377
14. Jörg M, Plehn JE, Kristen M, Lander M, Walz L, Lietz C, Wijns J, Pichot F, Rojas-Charry L, Martin W, Ruffini KM, Kreim N, Gerber N, Motorin S, Endres Y, Rossmanith K, Methner W, Helm A, Friedland M, K (2024) N1-methylation of adenosine (m1A) in ND5 mRNA leads to complex I dysfunction in Alzheimer's disease. Mol Psychiatry. https://doi.org/10.1038/s41380-024-02421-y
15. Kisler K, Nelson AR, Montagne A, Zlokovic BV (2017) Cerebral blood flow regulation and neurovascular dysfunction in Alzheimer disease. Nat Rev Neurosci 18:419–434. https://doi.org/10.1038/nrn.2017.48
16. Korte N, Nortley R, Attwell D (2020) Cerebral blood flow decrease as an early pathological mechanism in Alzheimer's disease. Acta Neuropathol. https://doi.org/10.1007/s00401-020-02215-w
17. Li R, Thinh N, Yingchun PTZ (2019) Dynamic cortical connectivity alterations associated with Alzheimer's disease: An EEG and fNIRS integration study. Neuroimage Clin 21:1–11
18. Mamelak M (2023) The Alzheimer's Disease Brain, Its Microvasculature, and NADPH Oxidase. J Alzheimer's Disease 1–10. https://doi.org/10.3233/jad-230415
19. Monzio Compagnoni G, Di Fonzo A, Corti S, Comi GP, Bresolin N, Masliah E (2020) The Role of Mitochondria in Neurodegenerative Diseases: The Lesson from Alzheimer's Disease and Parkinson's Disease. Mol Neurobiol. https://doi.org/10.1007/s12035-020-01926-1
20. Oldag A, Neumann J, Goertler M, Hinrichs H, Heinze HJ, Kupsch A, Sweeney-Reed CM, Kopitzki K (2016) Near-infrared spectroscopy and transcranial sonography to evaluate cerebral autoregulation in middle cerebral artery steno-occlusive disease. J Neurol 263:2296–2301. https://doi.org/10.1007/s00415-016-8262-5
21. Raz L, Knoefel J, Bhaskar K (2016) The neuropathology and cerebrovascular mechanisms of dementia. J Cereb Blood Flow Metab. https://doi.org/10.1038/jcbfm.2015.164
22. Scholkmann F, Tachtsidis I, Wolf M, Wolf U (2022) Systemic physiology augmented functional near-infrared spectroscopy: a powerful approach to study the embodied human brain. Neurophotonics 9:1–24. https://doi.org/10.1117/1.NPh.9.3.030801

23. Srinivasan S, Butters E, Collins-Jones L, Su L, O'Brien J, Bale G (2023) Illuminating neurodegeneration: a future perspective on near-infrared spectroscopy in dementia research. https://doi.org/10.1117/1.nph.10.2.023514. Neurophotonics 10
24. Swerdlow RH (2018) Mitochondria and Mitochondrial Cascades in Alzheimer's Disease. J Alzheimer's Disease. https://doi.org/10.3233/JAD-170585

Figures

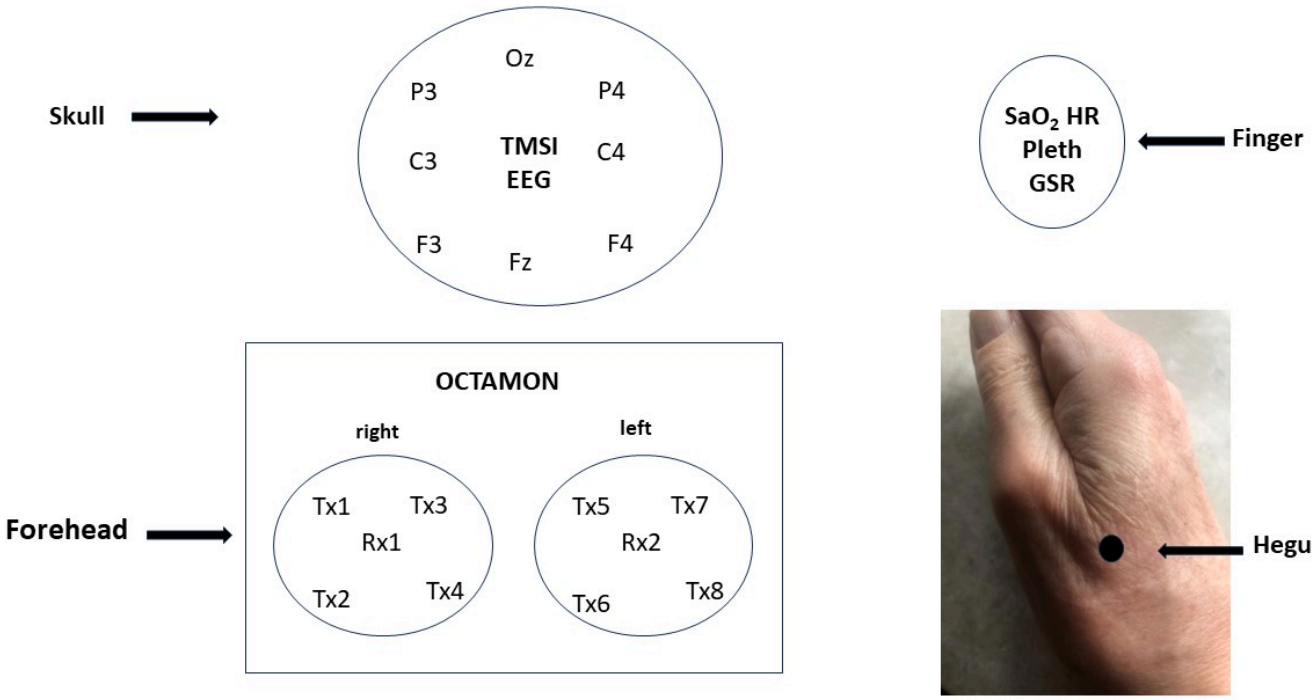

Figure 1

illustrates the experimental setup of the brain OctaMon NIRS. The setup includes Tx1–Tx8 diodes, which emit light at wavelengths of 751 nm and 843 nm. The emitted light passes through the brain tissue by reflection and is subsequently captured by Rx1 and Rx2. This configuration allows for the simultaneous measurement of oxygenated (O_2Hb) and deoxygenated (HHb) blood levels. Additionally, bipolar EEG signals (F3-F4, C3-C4, Fz-Oz, P3-P4), the GSR, the HR, and peripheral blood oxygen saturation (SaO2) were monitored. Furthermore, blood volume changes were assessed using photoplethysmography (Pleth) techniques.

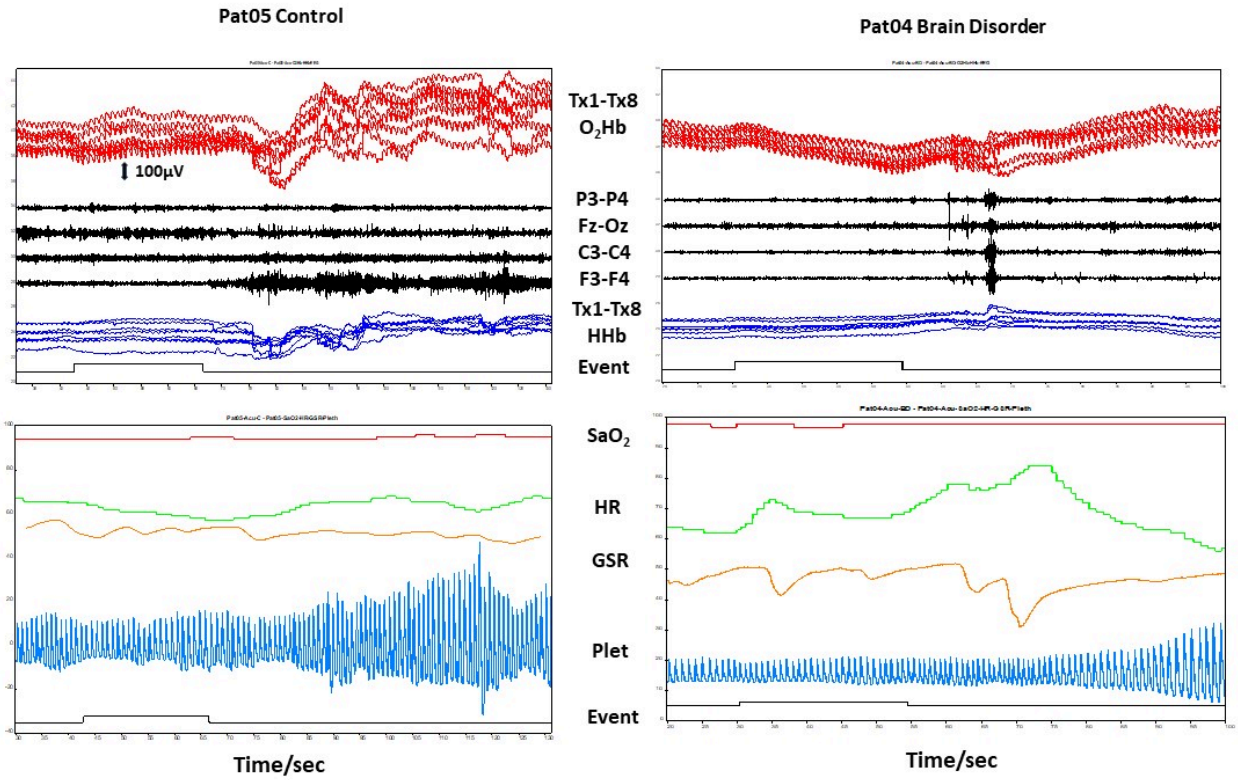

Figure 2

the left side shows the O_2Hb and HHb reactions to right-hand Hegu acupuncture (event) for 20 seconds at Pat05 CP. This was measured using frontal head fNIRS of Tx1-Tx8 O_2Hb (red) and HHb (blue), along with simultaneous registrations of bipolar EEGs (black, F3-F4, C3-C4, Fz-Oz, P3-P4). The figure below illustrates the changes in SaO_2, HR, GSR, and platelet count during the same time period.

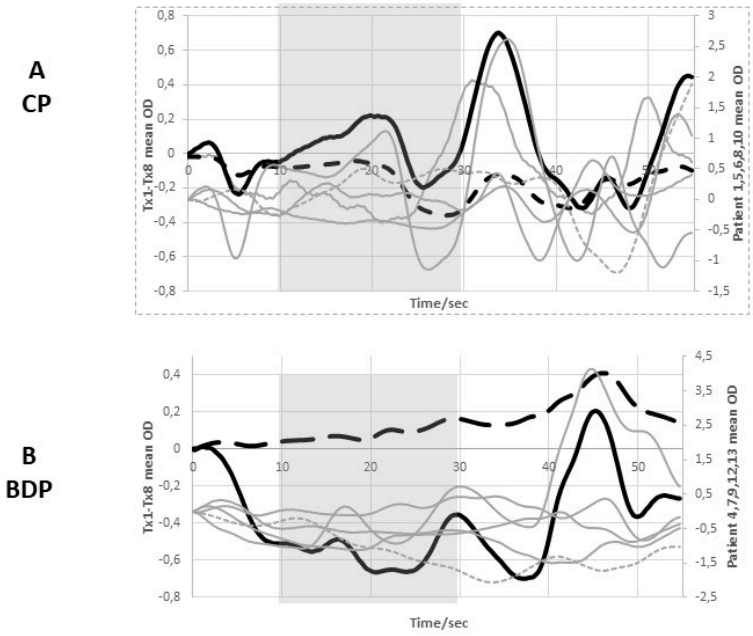

Figure 3

shows the O_2Hb reactions of channels T1-Tx8 from 5 CPs to acupuncture for 20 s (shaded area) as gray lines. The values of control patient 05 are shown as dotted gray lines. The mean O_2Hb reaction is shown as a solid black bold line, whereas the mean HHb reaction is shown as a broken black bold line. Figure 3B shows the single O_2Hb reactions of channels T1-Tx8 of 5 BDPs to acupuncture for 20 s (shaded area) as gray lines. The values for BD patient 04 are shown as dotted gray lines. The mean O_2Hb reaction is shown as a solid black bold line, whereas the mean HHb reaction is shown as a broken black bold line.

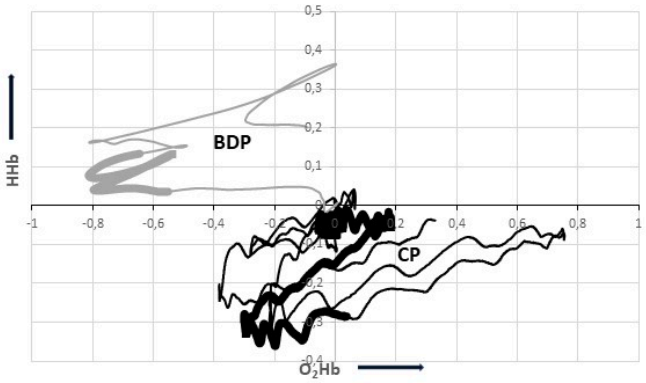

Figure 4

shows the differences in brain oxygen supply in response to Hegu acupuncture between CPs and BDPs. The x-axis shows the O_2Hb, and the y-axis shows the corresponding HHb optical density (OD) changes as the mean value of 5 CPs (black solid line) and 5 BDPs (gray solid line). The bold part of the lines represents the time period of 20 s of acupuncture.

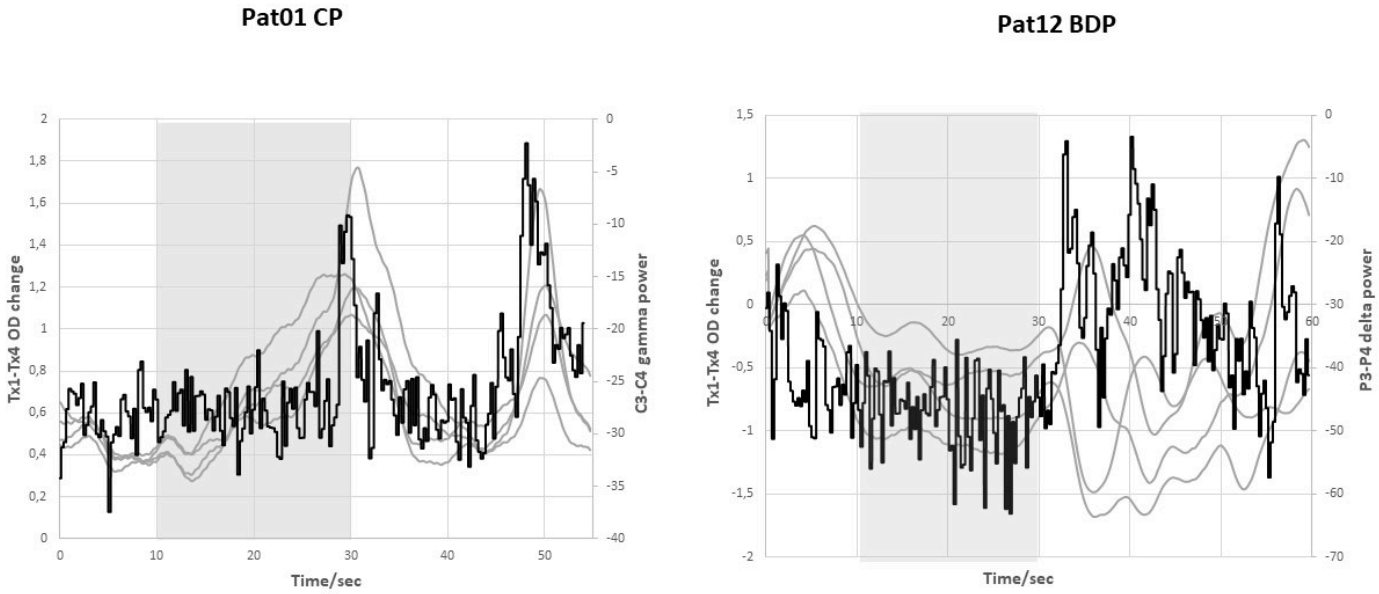

Figure 5

shows on the left side the increasing Tx1-Tx8 O_2Hb reaction (gray lines) in response to acupuncture (shaded area) of 1 CP (Pat01) as well as the nearly parallel reaction of the gamma power of the EEG C3-C4 recording. On the right-hand side, gray lines show the decreasing Tx1-Tx8 O_2Hb reaction in response to acupuncture (shaded area) of 1 BDP (Pat12) as well as the nearly parallel reaction of the gamma power of the EEG P3-P4 recording.

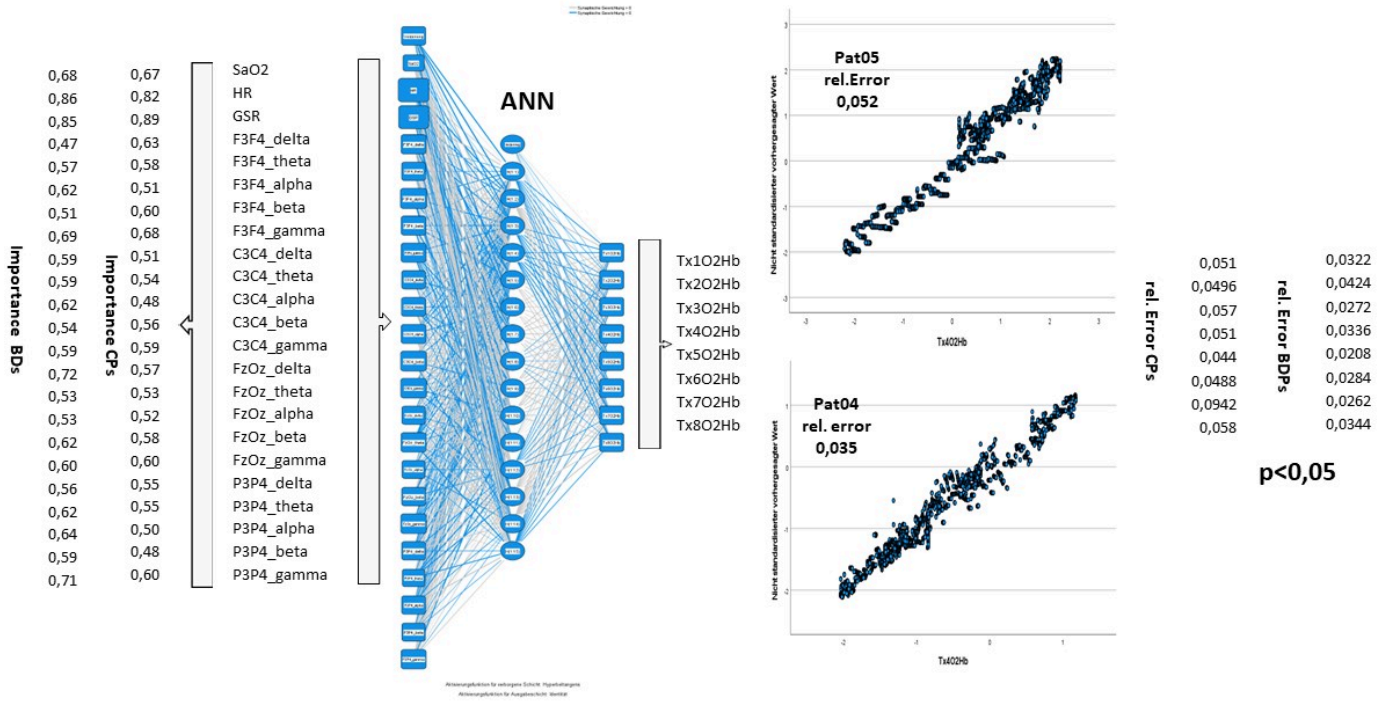

Figure 6

shows the ANN setup for analyzing the relative importance of 23 measured explanatory parameters (left side of the blue part) for estimating the Tx1-Tx8 O_2Hb- and HHb-dependent variables (right side of the blue part) under acupuncture using one hidden neural layer with 18 units (blue middle part). The left panel shows the 23 explanatory parameters measured and calculated during the experiment and their relative importance used for recalculation. The thickness of the blue lines in the middle between the 23 explanatory parameters and the Tx1-Tx8 O_2Hb variable increases with increasing relative importance. The diagrams on the right side of the blue part show the linear relationship between the measured and ANN-recalculated Tx4 O_2Hb of 1 CP (Pat05) and Tx4 O2Hb values for 1 BDP (Pat04) and the corresponding relative error. The relative error of calculation for the Tx1-Tx8 O_2Hb BDP recordings was significantly lower than that for the Tx1-Tx8 O_2Hb CP recordings.

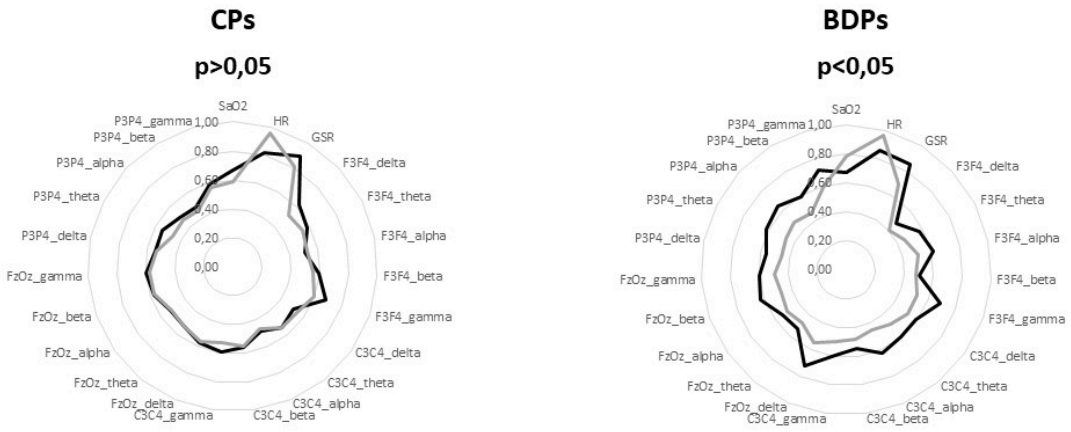

Figure 7

shows a net diagram of the relative importance of 23 parameters for recalculating fNIRS O_2Hb (black line) and HHb changes (gray line) upon Hegu acupuncture for 20 s for 5 CPs (left side) and 5 BDPs (right side).

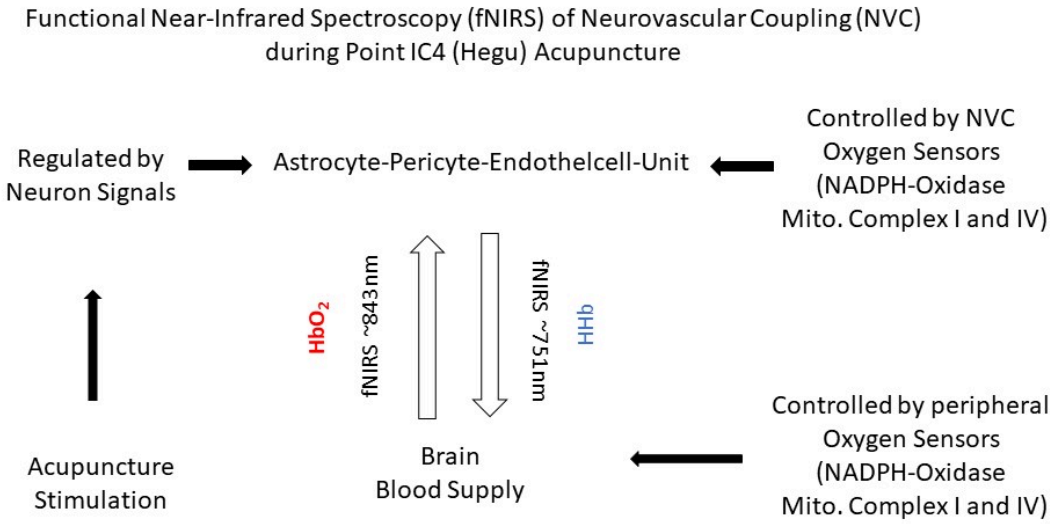

Figure 8

shows that NVC is regulated by neuronal activity signals and controlled by oxygen sensors based on the activity of NADPH oxidase, the activity of mitochondrial complexes I and IV and the blood supply in the brain controlled by peripheral oxygen sensors (NADPH oxidase and mitochondrial complexes I and IV, as described for the carotid body oxygen sensor).